

Design, fabrication and characterization of indefinite metamaterials of nanowires

BY JIE YAO¹, YUAN WANG¹, KUN-TONG TSAI², ZHAOWEI LIU³,
XIAOBO YIN^{1,4}, GUY BARTAL¹, ANGELICA M. STACY⁵, YUH-LIN WANG^{2,6}
AND XIANG ZHANG^{1,4,*}

¹*National Science Foundation (NSF) Nanoscale Science and Engineering Center (NSEC), University of California, 5130 Etcheverry Hall, Berkeley, CA 94720–1740, USA*

²*Institute of Atomic and Molecular Sciences, Academia Sinica, PO Box 23-166, Taipei 10617, Taiwan, Republic of China*

³*Department of Electrical and Computer Engineering, University of California, San Diego, La Jolla, CA 92093, USA*

⁴*Materials Sciences Division, Lawrence Berkeley National Laboratory, 1 Cyclotron Road, Berkeley, CA 94720, USA*

⁵*Department of Chemistry, University of California, Berkeley, CA 94720, USA*

⁶*Department of Physics, National Taiwan University, Taipei 10617, Taiwan, Republic of China*

Indefinite optical properties, which are typically characterized by hyperbolic dispersion relations, have not been observed in naturally occurring materials, but can be realized through a metamaterial approach. We present here the design, fabrication and characterization of nanowire metamaterials with indefinite permittivity, in which all-angle negative refraction of light is observed. The bottom-up fabrication technique, which applies electrochemical plating of nanowires in porous alumina template, is developed and demonstrated in achieving uniform hyperbolic optical properties at a large scale. We developed techniques to improve the uniformity and to reduce the defect density in the sample. The non-magnetic design and the off-resonance operation of the nanowire metamaterials significantly reduce the energy loss of electromagnetic waves and make the broad-band negative refraction of light possible.

Keywords: metamaterial; nanowire; porous alumina; bottom-up fabrication

1. Introduction

Our ability of versatile, but precise control and manipulation of light has been greatly enhanced ever since the concept of metamaterials was introduced. With artificially designed subwavelength structures, metamaterials have been applied to achieve a great variety of unprecedented optical effects such as negative refraction [1–5], superlens [6,7], invisible cloak [8–14] and more generally

*Author for correspondence (xzhang@me.berkeley.edu).

One contribution of 9 to a Theo Murphy Meeting Issue ‘Metallic metamaterials and plasmonics’.

transformational optics [15,16]. In the 1960s, Veselago suggested that negative refraction of light can be found in a material with simultaneous negative permittivity and permeability [17]. It took more than three decades before researchers were able to design metamaterials to achieve such an intriguing effect [1–3]. Soon after that, various designs have been explored, and negative refraction in metamaterials has been experimentally demonstrated from microwave to optical frequencies. However, many of the metamaterial properties were made possible by the resonance of the magnetic component of electromagnetic waves, which is intrinsically narrow band and suffers substantial energy loss, especially at optical frequencies.

An indefinite medium with a metallic nanowire array embedded in a dielectric matrix, on the other hand, does not rely on magnetic resonance and works over a broad range of frequency with much lower material loss [4,18]. Such an anisotropic material has a negative electric permittivity along the nanowires and a positive permittivity perpendicular to the wires, i.e. indefinite permittivity, resulting in a hyperbolic dispersion with the ability for negative refraction of light. To operate such a metamaterial at optical frequencies, fabrication techniques to produce high-aspect-ratio metallic nanowires at large scale are mandatory. By electrochemical deposition of silver in self-organized porous alumina templates, we demonstrate the efficient fabrication of indefinite metamaterials with designed geometry parameters. The low-energy loss of nanowire metamaterials enables the optical applications of bulk materials much thicker than the working wavelength. All-angle negative refraction of visible light in such composite materials was observed [4]. Here, we present detailed studies on the design, structure fabrication and characterization of the indefinite metamaterials made by metallic nanowire arrays embedded in a dielectric host.

2. Physics of indefinite metamaterials

To understand how the indefinite permittivity of a material leads to negative refraction [18,19], let us first consider the transverse magnetically (TM) polarized electromagnetic waves propagating in a uniaxial anisotropic material. The dispersion relation of such TM waves is given by

$$\frac{k_v^2}{\varepsilon_p} + \frac{k_p^2}{\varepsilon_v} = \frac{\omega^2}{c^2},$$

where c is the speed of light in vacuum, k_v and ε_v are wave vector and permittivity components perpendicular to the optical axis, respectively, k_p and ε_p are parallel to the optical axis and ω is the angular frequency of light. When the permittivity components ε_p and ε_v have opposite signs, the above dispersion relation results in a hyperbolic iso-frequency contour as shown in [figure 1a](#). The energy flow in the materials, indicated by the direction of Poynting vector \mathbf{S} , undergoes a negative refraction as it is normal to the iso-frequency contour and flows away from the interface. On the contrary, the refracted wave vector, the direction of the phase velocity, is positive given that the tangential component of the wave vector at the interface has to be conserved.

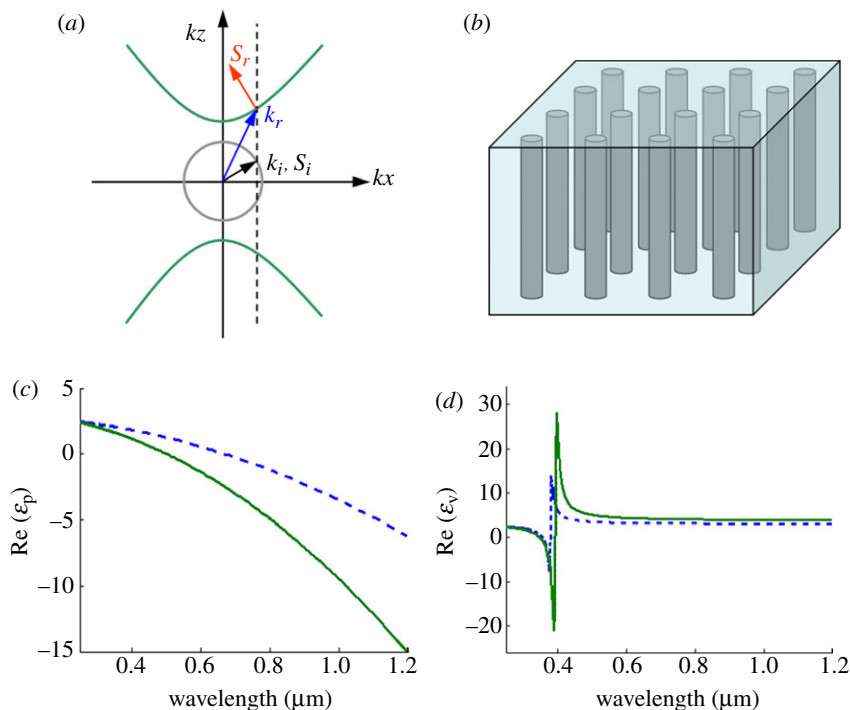


Figure 1. (a) Hyperbolic iso-frequency contour for an anisotropic indefinite medium when $\epsilon_v > 0$ and $\epsilon_p < 0$, and circular iso-frequency contour for an isotropic medium such as air. For an oblique incidence from air, the Poynting vector is negatively refracted inside the medium, although the wave vector undergoes positive refraction. (b) A typical realization of an indefinite metamaterial composed of an array of parallel metallic nanowires embedded in a dielectric matrix. (c, d) ϵ_p and ϵ_v values (real parts) as functions of wavelength in a vacuum with two different filling ratios of 0.1 (dashed line) and 0.2 (solid line). Alumina permittivity $\epsilon = 2.4$ was used [20], and the data for permittivity of silver were obtained from literature [21]. (Online version in colour.)

A typical realization of the indefinite metamaterial is composed of arrays of parallel metallic nanowires such as silver, gold, etc. embedded in a dielectric matrix. The indefinite optical properties of the nanowire metamaterials are briefly summarized in figure 1. Figure 1b is a schematic illustration of the nanowire metamaterial. As long as the period of the nanowire array is much smaller than the wavelength of interest, the structure can be effectively characterized as a homogeneous uniaxial anisotropic material with a permittivity parallel to wires (ϵ_p) and a permittivity vertical to wires (ϵ_v) [18,22],

$$\begin{aligned}\epsilon_p &= p\epsilon_m + (1-p)\epsilon_d, \\ \epsilon_v &= \frac{[(1+p)\epsilon_m + (1-p)\epsilon_d]\epsilon_d}{(1-p)\epsilon_m + (1+p)\epsilon_d},\end{aligned}\quad (2.1)$$

where p is the filling ratio of metal and ϵ_m and ϵ_d are the permittivity of the metal and dielectric, respectively. As shown in figure 1c,d, ϵ_p is negative, while ϵ_v keeps positive over a broad wavelength range from the visible to near-infrared. The

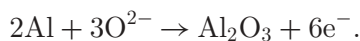
iso-frequency contour of light inside such a material is therefore hyperbolic and fulfils the requirement for achieving negative refraction. With the same composing materials, the optical properties of such material can be fine tuned by a single parameter of filling ratio p , as shown in figure 1. A smaller filling ratio has less metal inclusion and therefore results in relatively small Ohmic loss. On the other hand, a large filling ratio is favourable in order to achieve the indefinite medium at higher frequency, as shown in figure 1c. The unique tunability of the structure allows us to customize the nanowire design for different applications. Considering the above restrictions and our fabrication capability, we chose a filling ratio of 0.18–0.2 in fabrication for the demonstration of the negative refraction of light with broad-band wavelength.

3. Indefinite metamaterial fabrication

Nanowire metamaterials take advantage of the bottom-up fabrication technique based on the electrochemical deposition of silver nanowires inside self-assembled porous alumina template. With this mean, the metallic nanowires, a few tens of nanometres in diameter and an aspect ratio greater than 1000, can be efficiently fabricated at large scale, which are not achievable with any other traditional top-down approaches. Techniques such as two-step anodization and pre-pattern induced self-assembly are employed to further improve the optical properties of the indefinite medium and make it suitable for photonic applications such as negative refraction.

Self-ordered nanoporous materials such as molecular sieves, track-etched polymer, nanochannel array glass, radiation track etched mica, block copolymers and anodic aluminium oxide (AAO) have been utilized as the mask or the template for nanostructure fabrication [23]. However, the AAO-based template has great advantages over the others due to the well-ordered pore distribution, high pore density and the high aspect ratio of pores. Moreover, the thickness, diameter and pitch of the pores can be precisely tuned during fabrication, which makes the optical property of the final material controllable. In this work, silver is chosen as the metallic nanowire material for its lowest loss at the optical frequencies, and alumina is directly used as the dielectric component in the indefinite medium.

The AAO templates are prepared by electrochemical anodization of aluminium in an acidic solution. Anodization parameters, such as voltage, current density, electrolyte temperature and composition, are all adjustable and can be tuned for fabrication of a suitable template with desired distribution, size and length of the pores. The formation of alumina starts from the surface of the aluminium metal facing the electrolyte. During the anodization process [24,25], oxidation of aluminium metal occurs at the metal/oxide interface by the migration of oxygen containing ions (O^{2-} or OH^-) from the electrolyte by the following reaction:



The porous structure indicates a dissolution process in part of the aluminium oxide layer. It is caused mainly by the electric-field-enhanced reaction of the

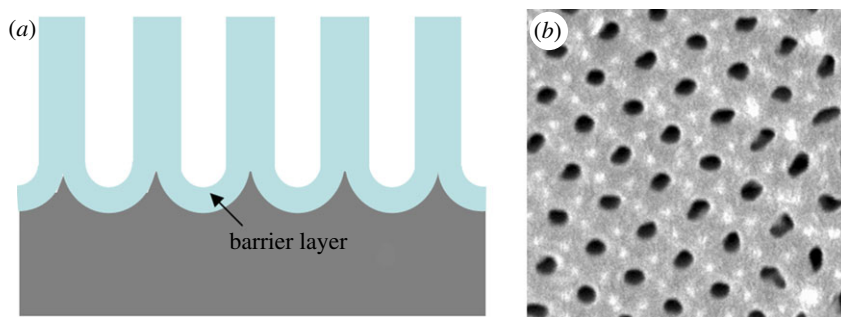
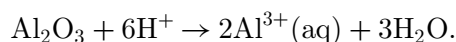


Figure 2. (a) Schematic of the vertical cross section of the porous alumina membrane formed on top of an aluminium substrate. The curved layer at the bottom of each pore is the barrier layer. (b) Scanning electron microscope (SEM) image of the porous alumina template (top view). (Online version in colour.)

formed oxide layer,



The positions of the pores are induced by the concaves at the top surface of the aluminium before anodization. The oxidation of aluminium and the dissolution of the oxide at the bottom of each pore are in equilibrium, hence a straight pore can be formed all the way into the metal layer (see figure 2). The formation of pores also involves the interaction among them. The growth competition results in a self-organized process and adjusts the relative position of adjacent pores, thus an ordered hexagonal pore array can be formed [26].

Various acids can be used for aluminium anodization, and the geometric feature of pores varies significantly with the electrolytes used. Pore size and distance between pores can be further controlled using an applied voltage between the electrodes. Generally speaking, they become larger as the anodization voltage increases [27]. Here, we use 0.2 M oxalic acid in an ice water bath with 40 V bias, which achieves approximately 110 nm pitch and approximately 55 nm pore size over a large area with a regular pore shape. The filling ratio p is in the range 0.18–0.2, as designed.

A better ordered nanopore array can be achieved using a two-step anodization process [26], since the development of the nanopores in AAO templates is guided by the appropriate texture of the surface at the initial stage of anodization. High purity aluminium foil (99.9995%, Alfa Aesar) was first mechanically polished and degreased with acetone, then put into 0.2 M oxalic acid as an anode for the first anodization step. The oxidized layer was then removed in a mixture of H_3PO_4 and H_2CrO_4 , leaving a regular array of dips on the metal surface due to the self-organizing mechanism. A second anodization is then applied to achieve AAO templates with the desired thickness. With the two-step method, pore sizes and distances between the pores in the final template are much more controllable and uniform.

After the anodization process, the sample was immersed in a saturated solution of Hg_2Cl_2 to remove the residual aluminium. The barrier layer at the bottom of the template was then removed in diluted H_3PO_4 at room temperature. After the removal of a barrier layer, a silver seed layer was deposited (EB3, BOC Edwards)

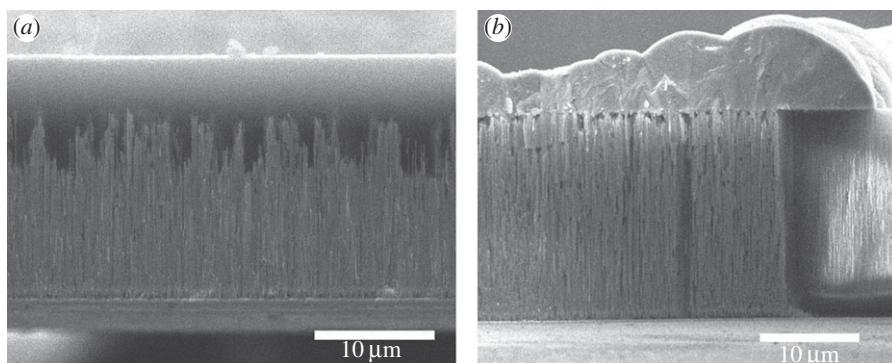


Figure 3. Cross-sectional view of an AAO template after the growth of a silver nanowire using the electrochemical plating method. (a) The centre part of the sample. (b) Close to the edge of the same sample in (a), the boundary between the nanowire filled and empty parts can be seen. The nanowires grow faster at the edge than at the centre part, and overgrown silver forms a block on top of the sample.

on top of the template as a cathode and silver nanowires were subsequently electrochemically plated in the pores of an AAO template [28]. The electroplating process was performed in the electrolyte containing AgNO_3 , nitric acid and l-tartaric acid.

Since the growth rate of nanowires is usually much faster close to the edge of the sample than in the centre [29], when the longer nanowires grow out of the pores, they will start to conglomerate at the surface and form a block of silver metal, as shown in figure 3. The overgrown silver on the surface was removed by mechanical polishing. The polishing process should not stop until all the short nanowires show up since the pores that are not fully filled act as strong optical scattering centres.

The bottom-up method using the self-organized porous template greatly reduces the fabrication time and makes fine and high-aspect-ratio nanostructures achievable. On the other hand, as shown in the previous example, materials made with a bottom-up approach are usually not so uniform in the pore sizes, shapes and lattice regularity as those fabricated with top-down approaches, which makes the fabrication of materials with good optical quality a great challenge. In order to further improve the optical performance, it is critical to create pore arrays with high uniformity.

First, the optical response of the metamaterial is dictated by the filling ratio of the metal nanowire in the dielectric matrix, as we have shown in the theory. The non-uniform size of the pores causes the fluctuation of effective permittivity throughout the material, resulting in a material property deviated from design.

Second, non-uniformity also results in the variation of the thickness of the barrier layer during the anodization, making random size openings in the barrier-layer removal process, as shown in figure 4a. In order to make sure every pore is fully opened, the etching time needs to be increased, which usually results in the unexpected widening of pores that open earlier. Different pore diameters and barrier-layer opening sizes lead to different ion transportation rates during the electro-deposition process, which may result in a very short nanowire or even no nanowires in some pores. The pores without nanowires are optical defects

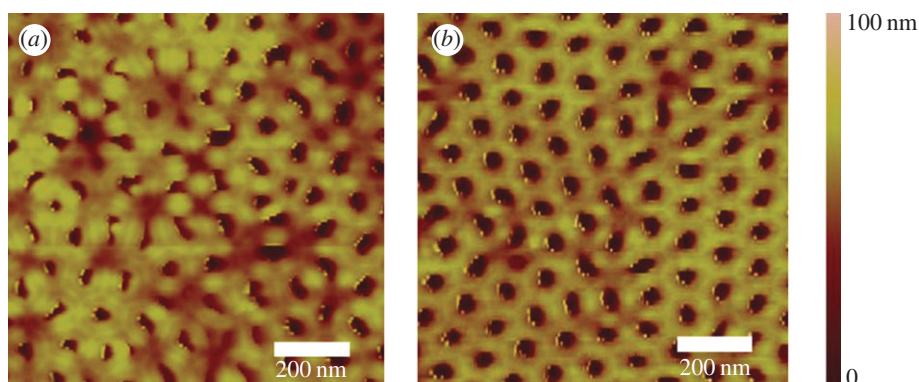


Figure 4. Atomic force microscope images of the template bottom surface morphology after removal of the barrier layers. The two samples are fabricated using the two-step anodization approach. First anodization time is (a) 5 and (b) 24 h, respectively. (Online version in colour.)

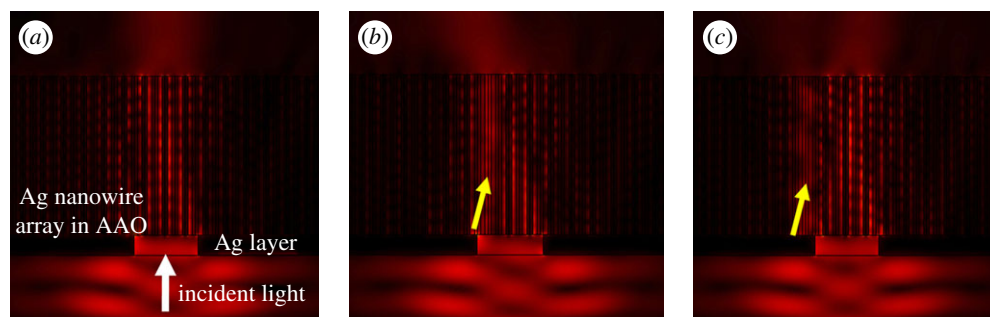


Figure 5. A three-dimensional simulation of light transmission through the anisotropic sample. The sample is a slab made of nanowire/AAO composite. The nanowires are along the vertical direction. Incident light with 660 nm wavelength is illuminated on the sample through a 600 nm slit cut in the silver layer covering the bottom surface of the slab. (a) Nanowire array without any missing nanowires and (b,c) a nanowire array with one missing nanowire, whose position is shown by an arrow. (Online version in colour.)

in the material, which induce unexpected scattering and create artefacts in the characterization process. Figure 5 depicts three-dimensional full wave simulation results showing the scattering effects caused by a single missing nanowire in a nanowire array where an open slit is cut through the silver seed layer. Light with wavelength 660 nm is incident from the bottom of the structure. Figure 5a is the result without any defects, while one nanowire is missing (shown by the arrows) in both figure 5b,c. When light is transmitted through the nanowire composite, a missing nanowire causes a strong distortion of the field distribution. Even when the missing nanowire is not in the slit region (figure 5c), the scattering is strong enough to result in an illusive field distribution. Figure 6 shows one example that the density of the defects in AAO is significantly affected by sample uniformity. Note that most defects occur at locations where the self-organized lattice is not well ordered.

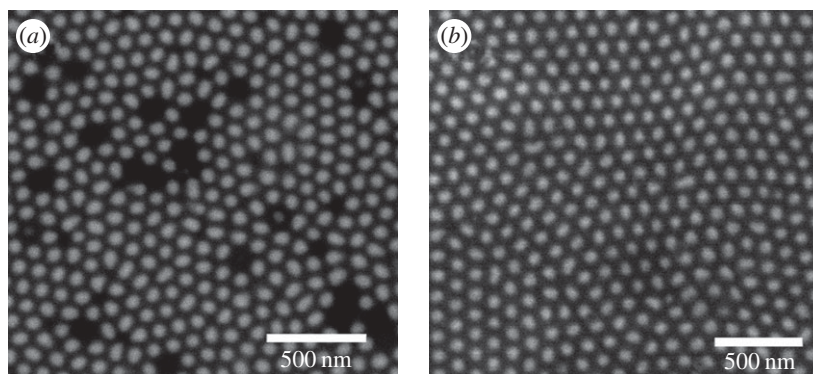


Figure 6. SEM images of two nanowire samples with different uniformity. It is clear that the pores in (a) are much less ordered than those in (b) [4], and therefore more defects can be found in it.

With the two-step anodization approach and the extended first anodization time, the ordering of the nanopore array can be significantly improved, which is also reflected in the uniform opening sizes of the barrier layer, as shown in figure 4b.

Other than the two-step anodization method, pre-pattern methods [30–33] can also be employed to achieve extremely narrow distributions on lattice spacing, pore size and thickness of the barrier layer. With the help of the fabulous uniformity of the template fabricated by pre-pattern methods for the following electroplating process, the reduction of missing nanowires and the precise control of the nanocomposite in the anisotropic metamaterials are then possibly obtained.

Here, we choose the focused-ion-beam (FIB) direct-write technique [31] for its effective guidance on the growth of high-aspect-ratio long-range-ordered nanochannel arrays and its flexibility on defining the tunable lattice spacing and exact position of every pore in the template. A commercial 50 keV Ga FIB with a diameter of approximately 10 nm and beam current of 10 pA is used to create arrays of hexagonally close-packed concaves on polished high-purity aluminium surfaces [31]. In the same principle as the two-step anodization method, the concaves will then induce the growth of ordered nanopores in the later anodization process. Given that the surface texture is compatible with the natural parameters for the self-ordering, the long-range-ordered nanopore array architecture can be expected to grow at the loci dictated by the pre-patterns. Figure 7a shows the scanning electron microscope (SEM) image of the FIB pre-patterned Al film, while Figure 7b is the nanopore array guided by the surface texture. Silver nanowires grown in an FIB pre-patterned template after anodization and barrier-layer removal create a nanowire array with an ideal order and high uniformity, as shown in figure 7c. Defects caused by the missing nanowire have been substantially reduced. Defect density is typically less than 0.05 per cent for samples with a pitch of approximately 110 nm and a nanowire diameter of approximately 50 nm. Notably, defects occur only at a few locations where the lattice is imperfect, which are negligible compared to the defects found in self-organized

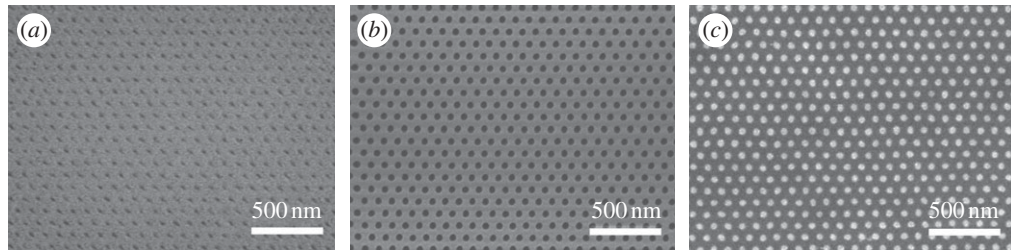


Figure 7. SEM images of FIB pre-patterned samples. (a) Pre-patterned Al film, (b) a nanopore array guided by the surface texture and (c) a silver nanowire array embedded in an AAO template fabricated by FIB pre-patterning.

nanochannels on AAO. The FIB pre-patterning of Al facilitates the fabrication of long-range-ordered AAO nanochannel arrays, which can be used as templates for growing arrays of nanowires exhibiting negative refraction without detrimental interference originated from defects on the arrays.

4. Optical measurements

As discussed in the previous section, an important consequence of the indefinite optical property is the negative refraction of light at the interface of the nanowire metamaterial and air. By utilizing a near-field scanning optical microscope (NSOM), optical measurements have been conducted to demonstrate the negative refraction ability of nanowire metamaterials.

The experimental setup is schematically illustrated in figure 8. The metamaterial slab comprising vertical aligned nanowires is mounted on the stage of the NSOM system. A $1\text{ }\mu\text{m}$ wide slit was etched through the silver seed layer using an FIB system (FIB, Strata 201XP, FEI), which can confine the light beam width within a certain propagation distance so that we are able to identify the direction of the refracted beam as shown in figure 9a. Such a slit can also serve as a one-dimensional object in order to demonstrate the imaging ability of slab lenses made of the nanowire metamaterials [34]. The slit is illuminated by a collimated laser beam at different incident angles, and the transmitted light is mapped by an apertured NSOM probe at the top surface of the metamaterial.

The incident angle of the light was controlled by shifting the collimated laser beam with a linear stage. The incident angle θ is determined by the equation $\theta = \arctan(x/f)$, where x is the shift of the beam and f is the focus length of the objective used to illuminate the sample. A polarizer was used to select transverse electric (TE) and TM modes of the incident light. When the polarization is parallel or perpendicular to the beam shift, TM or TE modes are excited inside the metamaterial, respectively. We marked the centre position of the transmitted beam under normal illumination as a reference. The lateral displacement of the beam x' at the output surface was determined by comparing the centre position of the beam with respect to the reference. The refraction angle inside the material θ' was consequently extracted by $\theta' = \arctan(x'/t)$, where t is the sample thickness.

The NSOM probe used to detect the output light is an optical fibre that was tapered and bent to 90° by a CO_2 laser beam. The tip apex was coated with 100 nm thick aluminium using e-beam deposition (Edwards EB3 E-beam

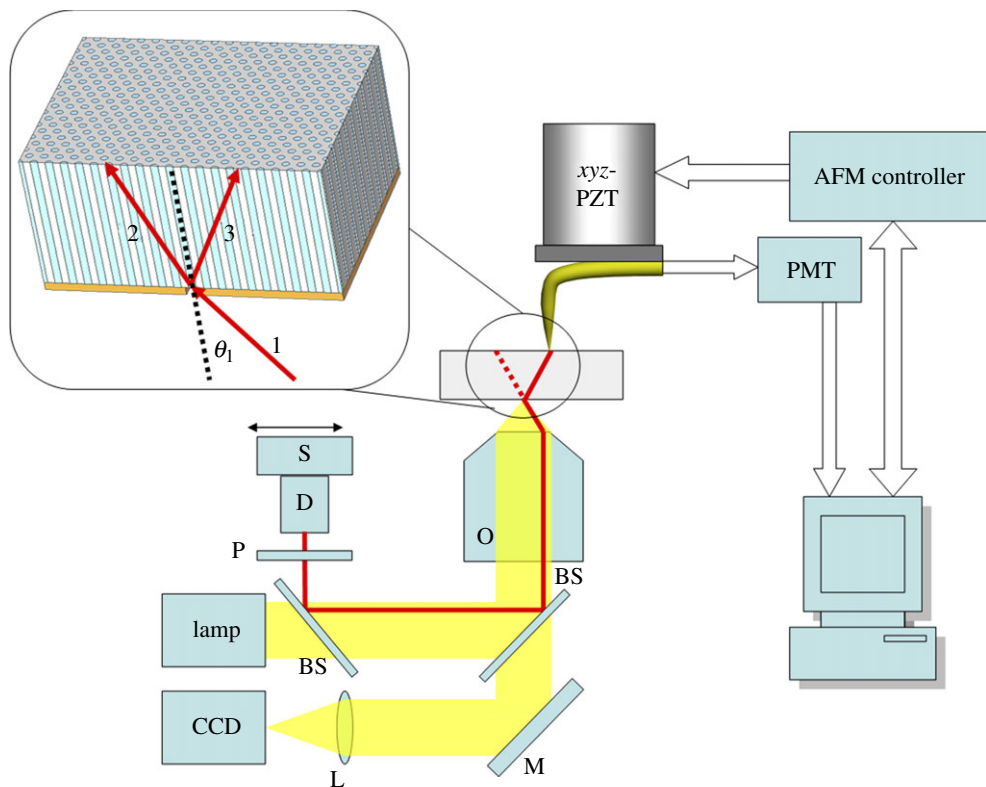


Figure 8. Schematic setup for negative refraction in silver nanowire metamaterials (BS, beam splitter; L, tube lens; M, mirror; O, objective; P, polarizer; xyz-PZT, piezo-scanner tunable in xyz directions; AFM, atomic force microscope; PMT, photomultiplier tube). The incident angle 1 is tuned by adjusting the position of the laser diode (D) with a one-dimensional stage (S). The inset illustrates a cross-sectional review of the light propagation of the TE mode (beam no. 2) and the TM mode (beam no. 3) inside the metamaterial. (Online version in colour.)

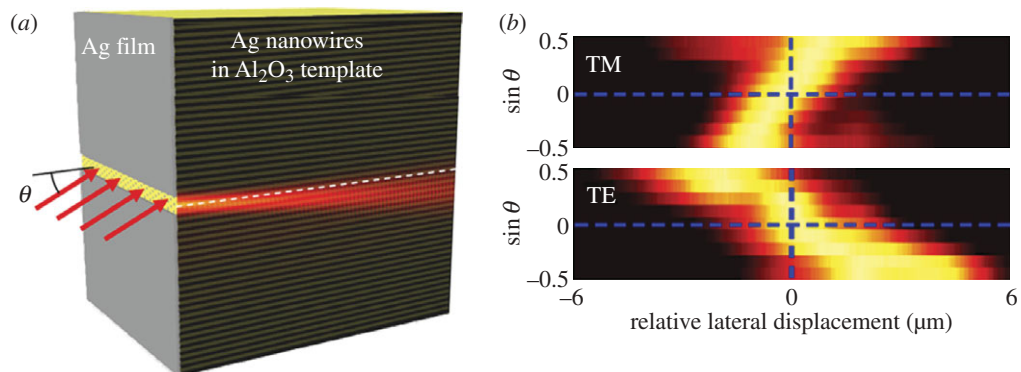


Figure 9. (a) Schematic picture of the light being negatively refracted at the air/metamaterial interface. The light beam is narrowed by a slit cut through the silver seed layer. (b) Experimental results of NSOM detected output light beam location as the incident angle varies. Upper half, TM-polarized light; lower half, TE-polarized light. (Online version in colour.)

Evaporator). Subsequently, the tip was milled using FIB milling (FEI Strata 201 XP) to form a sub-100 nm aperture at the probe apex. When positioned in close proximity to the sample surface with an atomic force microscope scanner (Bioscope, Digital Instruments), the light from the sample can be collected to form an image with subdiffraction resolution.

Figure 9a is a schematic showing the light path of a negatively refracted light in our experiments. A slit is cut on the 250 nm thick silver film. A light beam at 660 nm wavelength is transmitted through the slit and refracted to the negative direction at the air/metamaterial interface. Figure 9b is the combined results of a refracted light spot for different incident angles. The horizontal axis represents the lateral displacement of the output light. The output beam of normally incident light is set as the reference point and marked as zero on the axis. The vertical axes are the sines of various incident angles. When θ is negative, normal refraction dictates that the output beam has a positive displacement. However, it is clearly shown in the upper half of the figure that TM polarized light beams behave in the opposite way, which shows a negative refraction. In a control experiment, TE polarized light beams were positively refracted, as recorded in the lower half of figure 9b. Furthermore, negative refraction also occurs at the output interface of the sample, which leads to a focusing effect and forms an image of the slit at a distance from the output surface [34].

5. Conclusion

We have demonstrated the design, fabrication and optical characterization of an indefinite metamaterial composed of silver nanowires embedded in an alumina matrix, achieving an effective indefinite property in permittivity. The major challenge of creating such metamaterials with good optical quality was overcome by employing various techniques, including two-step anodization and the pre-patterning method, as well as parameter optimization to reduce the defect density. The approach is effective in producing high optical quality nanowire metamaterials with designed parameters at large scale. The indefinite optical properties were characterized by an NSOM system, and the negative refraction ability of the nanowire metamaterials was demonstrated. The experimental results in turn proved the validity of our theoretical framework and structure designs. An indefinite medium based on metallic nanowires has much lower material losses than other negative index materials because of its non-magnetic and off-resonance design. Such a bulk negative refractive material design has opened new possibilities in the fields of nanoscale optical imaging and lithography.

This work was supported by the US Army Research Office (ARO) MURI program 50432-PH-MUR and partly by the National Science Council (NSC 95-3114-P-001-007-MY3) of Taiwan and Academia Sinica of Taiwan.

References

- 1 Smith, D. R., Padilla, W. J., Vier, D. C., Nemat-Nasser, S. C. & Schultz, S. 2000 Composite medium with simultaneously negative permeability and permittivity. *Phys. Rev. Lett.* **84**, 4184–4187. (doi:10.1103/PhysRevLett.84.4184)

- 2 Pendry, J. B. 2000 Negative refraction makes a perfect lens. *Phys. Rev. Lett.* **85**, 3966–3969. (doi:10.1103/PhysRevLett.85.3966)
- 3 Shelby, R. A., Smith, D. R. & Schultz, S. 2001 Experimental verification of a negative index of refraction. *Science* **292**, 77–79. (doi:10.1126/science.1058847)
- 4 Yao, J., Liu, Z., Liu, Y., Wang, Y., Sun, C., Bartal, G., Stacy, A. M. & Zhang, X. 2008 Optical negative refraction in bulk metamaterials of nanowires. *Science* **321**, 930. (doi:10.1126/science.1157566)
- 5 Valentine, J., Zhang, S., Zentgraf, T., Ulin-Avila, E., Genov, D. A., Bartal, G. & Zhang, X. 2008 Three-dimensional optical metamaterial with a negative refractive index. *Nature* **455**, 376–379. (doi:10.1038/nature07247)
- 6 Fang, N., Lee, H., Sun, C. & Zhang, X. 2005 Sub-diffraction-limited optical imaging with a silver superlens. *Science* **308**, 534–537. (doi:10.1126/science.1108759)
- 7 Durant, S., Liu, Z., Steele, J. M. & Zhang, X. 2006 Theory of the transmission properties of an optical far-field superlens for imaging beyond the diffraction limit. *J. Opt. Soc. Am. B* **23**, 2383–2392. (doi:10.1364/JOSAB.23.002383)
- 8 Schurig, D., Mock, J. J., Justice, B. J., Cummer, S. A., Pendry, J. B., Starr, A. F. & Smith, D. R. 2006 Metamaterial electromagnetic cloak at microwave frequencies. *Science* **314**, 977–980. (doi:10.1126/science.1133628)
- 9 Cai, W., Chettiar, U. K., Kildishev, A. V. & Shalaev, V. M. 2007 Optical cloaking with metamaterials. *Nat. Photon* **1**, 224–227. (doi:10.1038/nphoton.2007.28)
- 10 Li, J. & Pendry, J. B. 2008 Hiding under the carpet: a new strategy for cloaking. *Phys. Rev. Lett.* **101**, 203901. (doi:10.1103/PhysRevLett.101.203901)
- 11 Liu, R., Ji, C., Mock, J. J., Chin, J. Y., Cui, T. J. & Smith, D. R. 2009 Broadband ground-plane cloak. *Science* **323**, 366–369. (doi:10.1126/science.1166949)
- 12 Valentine, J., Li, J., Zentgraf, T., Bartal, G. & Zhang, X. 2009 An optical cloak made of dielectrics. *Nat. Mater.* **8**, 568–571. (doi:10.1038/nmat2461)
- 13 Ergin, T., Stenger, N., Brenner, P., Pendry, J. B. & Wegener, M. 2010 Three-dimensional invisibility cloak at optical wavelengths. *Science* **328**, 337–339. (doi:10.1126/science.1186351)
- 14 Zhang, S., Genov, D. A., Sun, C. & Zhang, X. 2008 Cloaking of matter waves. *Phys. Rev. Lett.* **100**, 123002. (doi:10.1103/PhysRevLett.100.123002)
- 15 Pendry, J. B., Schurig, D. & Smith, D. R. 2006 Controlling electromagnetic fields. *Science* **312**, 1780–1782. (doi:10.1126/science.1125907)
- 16 Leonhardt, U. 2006 Optical conformal mapping. *Science* **312**, 1777–1780. (doi:10.1126/science.1126493)
- 17 Veselago, V. G. 1968 The electrodynamics of substances with simultaneously negative values of ϵ and μ . *Sov. Phys Usp.* **10**, 509. (doi:10.1070/PU1968v010n04ABEH003699)
- 18 Liu, Y., Bartal, G. & Zhang, X. 2008 All-angle negative refraction and imaging in a bulk medium made of metallic nanowires in the visible region. *Opt. Exp.* **16**, 15 439–15 448. (doi:10.1364/OE.16.015439)
- 19 Smith, D. R. & Schurig, D. 2003 Electromagnetic wave propagation in media with indefinite permittivity and permeability tensors. *Phys. Rev. Lett.* **90**, 077405. (doi:10.1103/PhysRevLett.90.077405)
- 20 Hornyak, G. L., Patrissi, C. J. & Martin, C. R. 1997 Fabrication, characterization, and optical properties of gold nanoparticle/porous alumina composites: the nonscattering Maxwell-Garnett limit. *J. Phys. Chem. B* **101**, 1548–1555. (doi:10.1021/jp962685o)
- 21 Johnson, P. B. & Christy, R. W. 1972 Optical constants of the noble metals. *Phys. Rev. B* **6**, 4370–4379. (doi:10.1103/PhysRevB.6.4370)
- 22 Podolskiy, V. A. & Narimanov, E. E. 2005 Strongly anisotropic waveguide as a nonmagnetic left-handed system. *Phys. Rev. B* **71**, 201101. (doi:10.1103/PhysRevB.71.201101)
- 23 Martin, C. R. 1994 Nanomaterials: a membrane-based synthetic approach. *Science* **266**, 1961–1966. (doi:10.1126/science.266.5193.1961)
- 24 Thompson, C. E. & Wood, G. C. 1983 Anodic films on aluminium. In *Treatise on materials science and technology*, pp. 205–329. New York, NY: Academic Press.
- 25 Li, F., Zhang, L. & Metzger, R. M. 1998 On the growth of highly ordered pores in anodized aluminum oxide. *Chem. Mater.* **10**, 2470–2480. (doi:10.1021/cm980163a)

- 26 Masuda, H. & Fukuda, K. 1995 Ordered metal nanohole arrays made by a two-step replication of honeycomb structures of anodic alumina. *Science* **268**, 1466–1468. (doi:10.1126/science.268.5216.1466)
- 27 Li, A. P., Muller, F., Birner, A., Nielsch, K. & Gosele, U. 1998 Hexagonal pore arrays with a 50–420 nm interpore distance formed by self-organization in anodic alumina. *J. Appl. Phys.* **84**, 6023–6026.
- 28 Lei, Y., Cai, W. & Wilde, G. 2007 Highly ordered nanostructures with tunable size, shape and properties: a new way to surface nano-patterning using ultra-thin alumina masks. *Progr. Mater. Sci.* **52**, 465–539. (doi:10.1016/j.pmatsci.2006.07.002)
- 29 Keyani, J. 2007 Electrodeposition and device incorporation of bismuth antimony nanowire arrays. PhD thesis, University of California Berkeley, USA.
- 30 Masuda, H., Yamada, H., Satoh, M., Asoh, H., Nakao, M. & Tamamura, T. 1997 Highly ordered nanochannel-array architecture in anodic alumina. *Appl. Phys. Lett.* **71**, 2770–2772. (doi:10.1063/1.120128)
- 31 Liu, C. Y., Datta, A. & Wang, Y. L. 2001 Ordered anodic alumina nanochannels on focused-ion-beam-prepatterned aluminum surfaces. *Appl. Phys. Lett.* **78**, 120–122. (doi:10.1063/1.1335543)
- 32 Krishnan, R. & Thompson, C. 2007 Monodomain high-aspect-ratio 2d and 3d ordered porous alumina structures with independently controlled pore spacing and diameter. *Adv. Mater.* **19**, 988–992. (doi:10.1002/adma.200601555)
- 33 Biring, S., Tsai, K., Sur, U. K. & Wang, Y. 2008 High speed fabrication of aluminum nanostructures with 10 nm spatial resolution by electrochemical replication. *Nanotechnology* **19**, 355302. (doi:10.1088/0957-4484/19/35/355302)
- 34 Yao, J., Tsai, K., Wang, Y., Liu, Z., Bartal, G., Wang, Y. & Zhang, X. 2009 Imaging visible light using anisotropic metamaterial slab lens. *Opt. Exp.* **17**, 22 380–22 385. (doi:10.1364/OE.17.022380)